Progress In Electromagnetics Research M, Vol. 109, 205–216, 2022

Multifunction Cross Polarization Converter Based on Ultra-Thin Transmissive Chiral Metasurface in C and X Bands

Jiayu Yu, Qiurong Zheng*, Bin Zhang, Huan Jiang, and Kun Zou

Abstract—Polarization is an essential feature of electromagnetic (EM) waves, and the variety and simplicity of polarization conversion have substantial demands in wireless systems. Metasurfaces, two-dimensional artificial electromagnetic structures, are emerging as novel modulation solutions for EM waves. In this work, a multifunction polarization converter based on a transmissive metasurface (MPC-TMS) is suggested. This planar structure is made up of a copper-clad dielectric substrate with top and bottom orthogonal slotted sheets joined by a metal via. With frequency selectivity, x- and y-linear cross-polarization transformations are efficiently achieved between 8.04–8.82 GHz (9.25%) and 7.04–9.07 GHz (25.19%), respectively. Meanwhile, the presented microstructure is capable of rotating a circularly polarized incident wave into its opposite handedness from 8.16 to 8.87 GHz (8.46%). Both peak transmission efficiency and the polarization conversion ratio exceed 0.95 simultaneously. In addition, resonance superposition and coupling effects are investigated to explain the operating mechanism. This microstructure not only has a simple construction with an ultra-thin thickness (0.06λ), but also reveals superiorities in bandwidth, transmission, and efficiency. To verify the above quadruple polarization conversion, measurement has been implemented, and the results are reasonably accordant with simulation, suggesting that the low-profile converter is conducive to future telecommunication design where polarization diversity is needed.

1. INTRODUCTION

Polarization is one of the main features of electromagnetic (EM) waves. Switching between vertical and horizontal polarizations, a transition from linear polarization (LP) to circular polarization (CP), and the handedness rotation of circular polarization are among the types of polarization conversion in EM waves [1–3]. In the microwave spectrum, suffering from bulky sizes and mass, conventional regulation approaches like metal columns [4], wire gratings [5], special substrate [6], which are equipped with reliable characteristics and stable conversion efficiency, have limitations in integrating into modern compact systems. Using sophisticated designs and elaborate structures, the researches of substrate integrated waveguide [7, 8] and Fabry-Pérot cavity [9, 10] have considerably increased the diversity of conversion functions and system compatibility during the last decade. However, the emergence of metasurface offers unique opportunities for EM modulation [11–18]. Metasurface, a kind of 2-dimensional formation, is acutely thin, light weight, and easy to artificially fabricated anisotropic materials. This meta-device, which is typically made up of a series of sub-wavelength meta-atoms arranged in a periodic pattern, allows for numerous unimaginable designs in EM wavefront manipulation [11], such as holographic imaging [12], perfect absorber [13], RCS reduction [15], and novel sensor applications [16–18].

In recent years, researches into the polarization of EM waves by metasurface have aroused considerable interest whether within the microwave region or in the optical spectrum [19–27]. In

Received 12 February 2022, Accepted 24 March 2022, Scheduled 6 April 2022
* Corresponding author: Qiurong Zheng (zqr1620@sina.com).
The authors are with the Information and Navigation College, Air Force Engineering University, Xi'an 710077, China.

ultrawideband from 12.4 to 27.96 GHz, a dual-V shaped metasurface in reflection-type can accomplish cross-polarization conversion for linearly polarized irradiated waves [20]. Similarly, devices that functioned as LP to CP have also been exposed [21, 22]. An effective polarization transformer based on reflective metasurface is studied [21], which can transform a linearly polarized light to linearly and circularly polarized lights over three frequency bands. A dynamic optical metaparticle based on a microelectromechanical system (MEMS) has been demonstrated recently, to offer steerable polarization conversion and amplitude manipulation of the reflected lights with quick responses [23]. Conversely, it is of great difficulty for metasurface in transmissive mode to actualize high-efficiency transmission and modulation due to involving both electric and magnetic resonances [24, 25, 28]. A planar chiral transmissive metamaterial has been displayed in [24] that works in triple-band and converts an LP wave into its cross-polarization component thanks for the symmetric coupling effects. Another meta-device, sheafed by bilayer gear-like metallic decoration, can reach nondispersive cross-polarization transmission of the normally incident linear and circular polarization waves [25]. However, there are few studies in C/X-band on single-layer transmissive metasurface that perform cross-polarization conversions for both LP and CP in the common frequency passband at the same time, which can contribute to the polarization conversion diversity.

In this work, a multifunction polarization converter based on a transmissive metasurface (MPC-TMS) in C/X-band is presented, which is constructed from two orthogonal slotted metallic patches on both sides and an ultra-thin dielectric substrate in the middle with no function material introduced. With frequency selectivity, a linearly polarized (x-/y-polarized) wave can be efficiently converted by this MPC-TMS into its cross-polarized (y-/x-polarized) counterpart from 8.04 to 8.82 GHz (9.25%) and from 7.04 to 9.07 GHz (25.19%), respectively. The schematic diagram is exhibited in Fig. 1. Due to its unique characteristics in the shared frequency region, the unit cell can simultaneously rotate right-hand polarization (RHCP) waves into left-hand polarization (LHCP) waves from 8.16 to 8.87 GHz (8.46%) with low insert loss, and vice versa. Resonance superposition and coupling effects are discussed to explore the physical mechanism and conversion performance. The unique side of this study is to have broader co-conversion bandwidth and lower thickness (0.06λ) along with higher peak transmission (0.95) than corresponding researches. A sample of the proposed metasurface is manufactured, and the measured results keep broadly in line with the simulation data, indicating that it has latent application in orbital angular momentum wave generation and satellite communications where polarization diversity is needed.

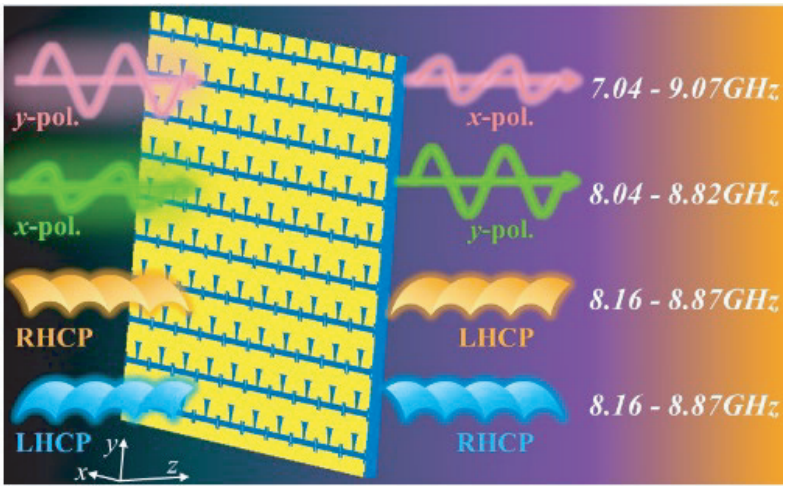

Figure 1. Schematic diagram of the presented MPC-TMS.

2. DESIGN AND DISCUSSION

2.1. Fundamental Theory Analysis

Considering a linearly polarized plane wave traveling through the z-axis of a metasurface unit under the Cartesian coordinates, the incident electric field vector can be split into two orthogonal elements, E_x^i and E_y^i. The relationship between the incident wave vector and the corresponding transmitted wave vector is explained by

$$E^t = \begin{bmatrix} E_x^t \\ E_y^t \end{bmatrix} = T_{lin} \cdot E^i = \begin{bmatrix} t_{xx} & t_{xy} \\ t_{yx} & t_{yy} \end{bmatrix} \begin{bmatrix} E_x^i \\ E_y^i \end{bmatrix} \tag{1}$$

where T_{lin} represents the Jones transmission matrix for linear polarization state. The co-polarization transmission coefficients are displayed as t_{xx} and t_{yy}, and the cross-polarization transmission coefficients are written as t_{yx} and t_{xy} of x- and y-polarizations, respectively.

Then, we denote the amplitude difference as $\Delta T = t_{xy} - t_{yx}$, and the corresponding phase difference is $\Delta\varphi = \varphi_{xy} - \varphi_{yx}$. Analogously, the Jones transmission matrix for circular polarization state can be described as [29]

$$T_{cir} = \begin{bmatrix} t_{RR} & t_{RL} \\ t_{LR} & t_{LL} \end{bmatrix} = \frac{1}{2} \begin{bmatrix} t_{xx} + t_{yy} + i(t_{xy} - t_{yx}) & t_{xx} - t_{yy} - i(t_{xy} + t_{yx}) \\ t_{xx} - t_{yy} + i(t_{xy} + t_{yx}) & t_{xx} + t_{yy} - i(t_{xy} - t_{yx}) \end{bmatrix} \tag{2}$$

where $t_{RR}(t_{LR})$ and $t_{LL}(t_{RL})$ are labeled as the co-polarization and cross-polarization transmission coefficients of RHCP and LHCP lights, respectively.

In order to attain a circularly polarized converter, the sum of the main diagonal needs to be zero while the sum of the sub-diagonal is not zero, i.e.,

$$t_{xx} + t_{yy} = 0 \tag{3a}$$

$$t_{xy} - t_{yx} = 0 \tag{3b}$$

An ordinary approach [3] for achieving such a function is to align the size of t_{xx} and t_{yy} and conform their phase difference to 180 degrees while suppressing cross-polarization components. Unfortunately, this conversion method for LP waves illuminated does not work.

Therefore, the following equation arising [28]

$$t_{xx} = t_{yy} = 0 \tag{4a}$$

$$t_{xy} = t_{yx} \neq 0 \tag{4b}$$

$$\Delta\varphi = \varphi_{t_{xy}} - \varphi_{t_{yx}} = 0 \tag{4c}$$

where t_{yx} and t_{xy} tend to be equal and non-zero ensuring a phase difference $\Delta\varphi = 0$. At the same time, when eliminating t_{xx} and t_{yy}, a perfect cross polarization converter is actualized. In other words, such a device is qualified to convert both linear and circular polarizations of incident waves into relevant cross-polarized counterparts in a common frequency passband, concurrently.

In general, the polarization conversion ratio (PCR) represents the element rate of the incident wave and the transmitted or reflected wave, revealing the availability of the polarization conversion. It can be indicated as

$$PCR = \frac{t_{ji}^2}{t_{ji}^2 + t_{ii}^2} \tag{5}$$

Practically, to meet the above ideal behavior and raise PCR, it is essential for this converter to deliver the amplitudes of diminished t_{xx} and t_{yy}, while the amplitudes and phase of t_{xy} and t_{yx} are as equal as possible.

2.2. Unit Cell Design and Simulation Results

The perspective view of the presented MPC-TMS is shown in Fig. 2(a). The middle layer, covered by two copper sheets, is chosen as F4BTMS220 whose relative dielectric constant and loss tangent are 2.2 and 0.0009, respectively. Identical in shape and orthogonal in direction, a combination of a Gaussian curve (GC) slot and a barbell-shaped (BS) slot is etched on the upper and lower metal patches. In Fig. 2(b),

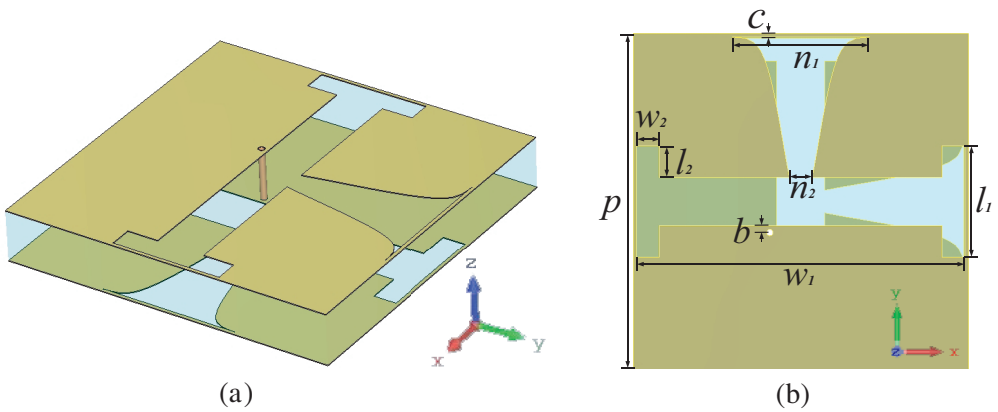

Figure 2. (a) Perspective view of the unit cell. (b) Geometry dimensions of the unit cell.

the width n_1 of the GC's bottom edge and the length w_1 of BS are 6 mm and 14.3 mm. 0.35 mm away from two BS slots, a copper via hole with a diameter d of 0.25 mm is employed to short the top and bottom metallic layers. To acquire a broader operating bandwidth, the other optimized geometric sizes of the unit cell are $w_2 = 1$ mm, $n_2 = 1$ mm, $l_1 = 4.83$ mm, $l_2 = 1.36$ mm, $c = 0.15$ mm, taking into account the processing technology. It is worth mentioning that the edge length p and total thickness h of the submitted periodical meta-atom are 14.6 mm and 2.2 mm, which are less than 0.43λ and 0.06λ, respectively. λ is the free-space wavelength at 8.7 GHz in the desired operating band. Therefore, the requirements of equipment miniaturization could be well satisfied by such a design.

The full-wave numerical simulations are implemented by CST Microwave Studio to investigate the performance of the MPC-TMS, and the simulated results are demonstrated in Fig. 3. The calculated transmission coefficients are shown in Fig. 3(a), where the amplitudes of cross-polarization in the shaded region are much larger than those of co-polarization. Reaching near-unity, 0.972 and 0.976 are the maximum values at 8.69 GHz for t_{yx} and t_{xy}, respectively. We consider the cross-polarization converter to have operated when cross transmission coefficient exceeds 0.8, whereas linear cross-polarization conversion is realized in 8.04–8.82 GHz (9.25%) and 7.04–9.07 GHz (25.19%) when the x and y linearly polarized waves are illuminated, respectively. Meanwhile, it is demonstrated in Fig. 3(b) that amplitude difference $\Delta T = t_{xy} - t_{yx}$ and phase difference $\Delta\varphi = \varphi_{xy} - \varphi_{yx}$ of the cross components are both approximately close to zero. As Eq. (4) expects, the territory of t_{LR} occurs in the overlapped fields of the t_{yx} and t_{xy} frequency range in Fig. 2(c), which tends to rotate the right hand circular polarization incident wave into left hand circular polarization transmissive wave from 8.16 to 8.87 GHz (8.46%) with a peak of 0.951 at 8.74 GHz. t_{RL} is not calculated because it is the same as t_{LR} according to Eq. (2). As Fig. 2(d) illustrated, the PCRs of LP and CP incident waves are extraordinarily high, exhibiting remarkable validity and purity in the aforementioned passband. Consequently, the manifold cross-polarization conversion based on the transmissive metasurface is realized.

2.3. Discussion of Resonance Superposition and Coupling Effects

In this work, the operating frequency is expected to be around 8.7 GHz, and the arrangement period p of meta-particles is chosen less than 0.43λ, in order to place more units on the finite array and boost the functional performance. A combination of a Gaussian curve (GC) slot and a barbell-shaped (BS) slot, as shown in Figs. 4(a) and (b), with the same geometrical size as shown in Fig. 2, plays a practical role in MPC-TMS. The two subassemblies are orthogonal to the corresponding partners on the upper and lower surfaces, respectively. Their transmission characteristics are shown in Figs. 4(d), (e). The resonant excitation caused by the GC slot permits the x-polarized wave to exhibit distinctive conversion and penetration properties in the passband compared to the rejection created by the y-polarized incident wave. Likewise, the BS slot, which attaches the top and bottom metal sheets through a via hole, produces a high-purity characteristic for y-polarized incident waves in frequency privilege and polarization rotation at 7.04–9.07 GHz. Thus, the motivation of the two makes the cross-conversion of linear polarization possible, while weak interaction exists. Owing to the resonance superposition effect,

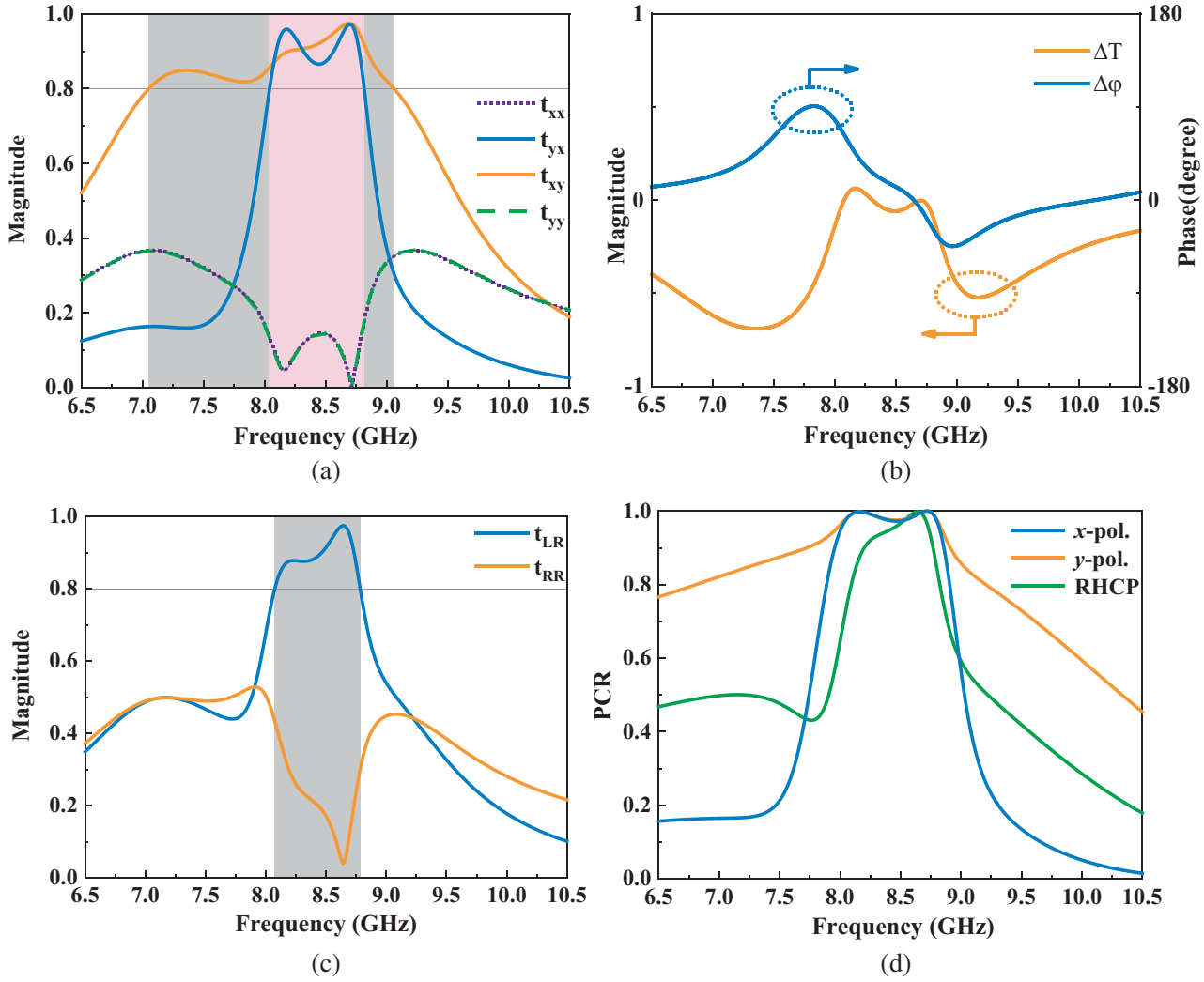

Figure 3. Simulated results. (a) Transmission coefficients, (b) amplitude difference and phase difference of linear polarization incidence. (c) Transmission coefficients of circular polarization incidence. (d) PCRs of linear and circular polarization incidence.

in association with Eq. (4), the circular polarization conversion function works when the transmissive cross-polarization coefficients draw near in phase, by optimizing structure parameters.

To further investigate the resonance mechanism of MPC-TMS, Fig. 5 exhibits the distributions of surface currents on the top and bottom sheets at 8.7 GHz.

When the x-polarized wave illuminates the structure, as shown in Fig. 5(a), strong induced currents are pronounced near the GC slot, especially concentrating around the bottom edge of the GC slot. Due to the aperture coupling of the upper and lower GC slots, significant currents are excited at the same location of the bottom layer, which is even in amplitude and orthogonal in orientation compared to the ones in the top layer. Concerning BS slots, in the contrary, invisible currents are assembling along with them, which means that the device functions similarly to a reflector. As a consequence, the incoming x-polarization of the electric field is turned to outgoing y-polarization while passing through the meta-atom.

For the y-polarized incidence, the unit cell in the passband also demonstrates the frequency selectivity of transmission and the polarization conversion characteristics. The current distribution in the upper and lower GC slots does not show a resonant state in Fig. 5(b), and the majority of the illuminated lights are reflected back. However, the opposite results can be detected that intense induced

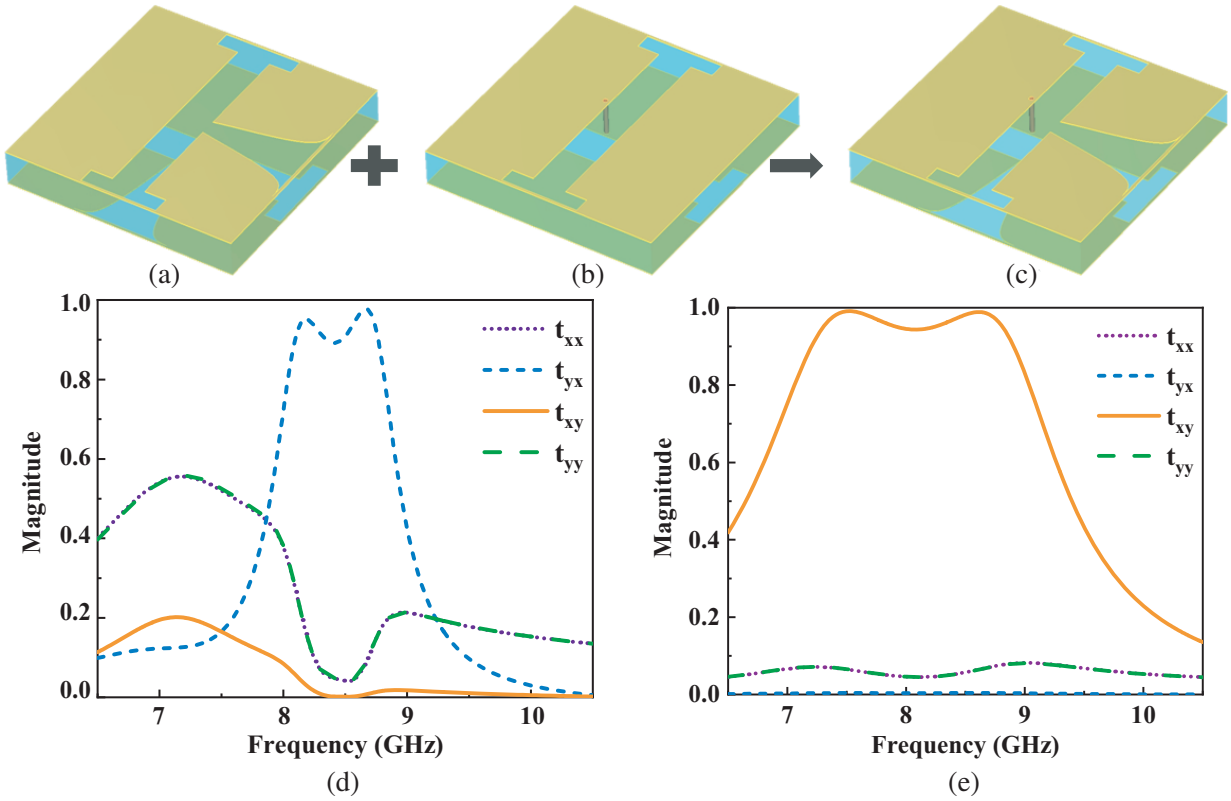

Figure 4. Perspective view of (a) GC slot, (b) BS slot and (c) the combination. Transmission characteristics of (d) GC slot, (e) BS slot.

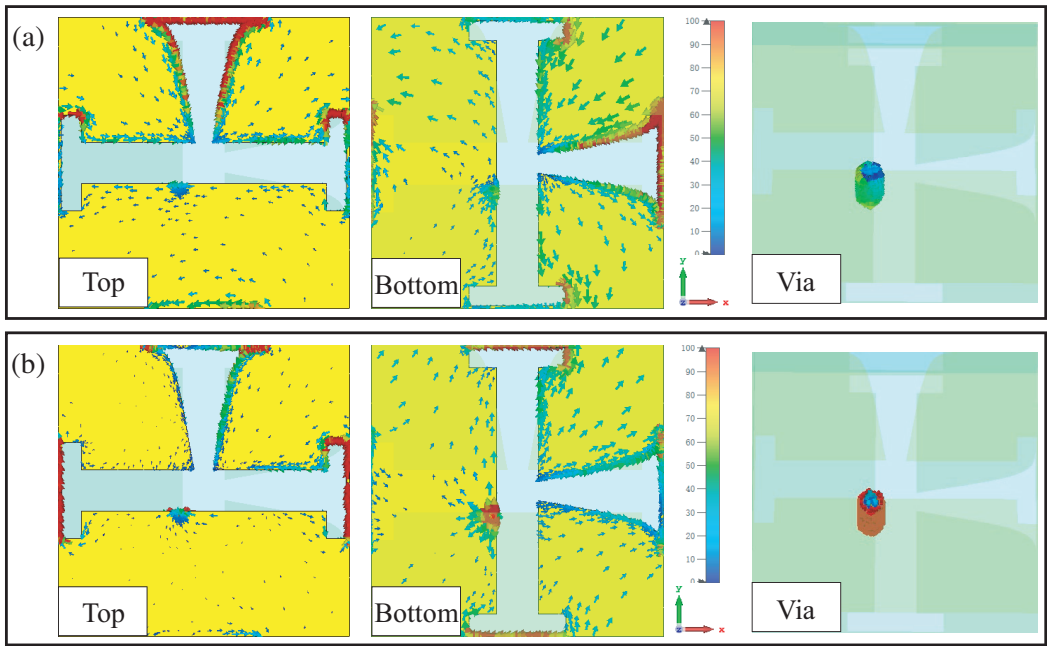

Figure 5. Surface currents distributions on the top layer, bottom layer and via hole of (a) x polarization incidence, (b) y polarization incidence.

currents are distributed at the edges of the BS slots. Similarly, strong currents are observed over the metal via hole. It is due to the orthogonal distributions of the BS slots on the top and bottom that the x-polarization lights tend to be radiated by the bottom patch, which is rotated over 90 degrees from y-polarization.

The antenna-coupler-antenna (ACA) model [19, 26, 30, 31] allows the operation mechanisms of the GC slot and the BS slot to be interpreted. With the frequency-selective characteristic, the ACA device consists of a receiving antenna, a coupling energy exchanger, and a radiating antenna. With respect to this design, the upper layer slot functions as a receiving antenna to recruit waves of a particular polarization while the lower layer slot acts as a radiation antenna to re-emit the lights of a rotated polarizer. Nevertheless, the coupling effects are diverse for the GC and BS slots. Engaging aperture coupling, for GC slots, coupling interaction appears in the shared slot area between the upper and lower slots. In the case of the BS slot, the coupling energy exchange mainly takes place in the copper via hole linking the layers. That is why significant currents concentrations have existed for y-polarized illuminated around the via structure, while it is not activated with the x-polarized waves incidence. Meanwhile, the conversion bandwidth of y-polarization is more expansive than that of x-polarization because of the direct connection of via hole. In fact, the service of this polarization converter is able to be realized in a wide range of microwave fields, where the cell structure varies in proportion to the wavelength.

2.4. Performance Effect of Dielectric Thickness and Oblique Incidence

Generally speaking, the dielectric thickness affects the performance of transmissive metasurface. Figs. 6(a), (b), (c) give a performance comparison of this multifunctional cross polarization converter at different thicknesses of h. On the one hand, for x-polarized incident waves, the polarization conversion function is always maintained in the range of 8.0–8.9 GHz, regardless of the variation of h from 1 mm to

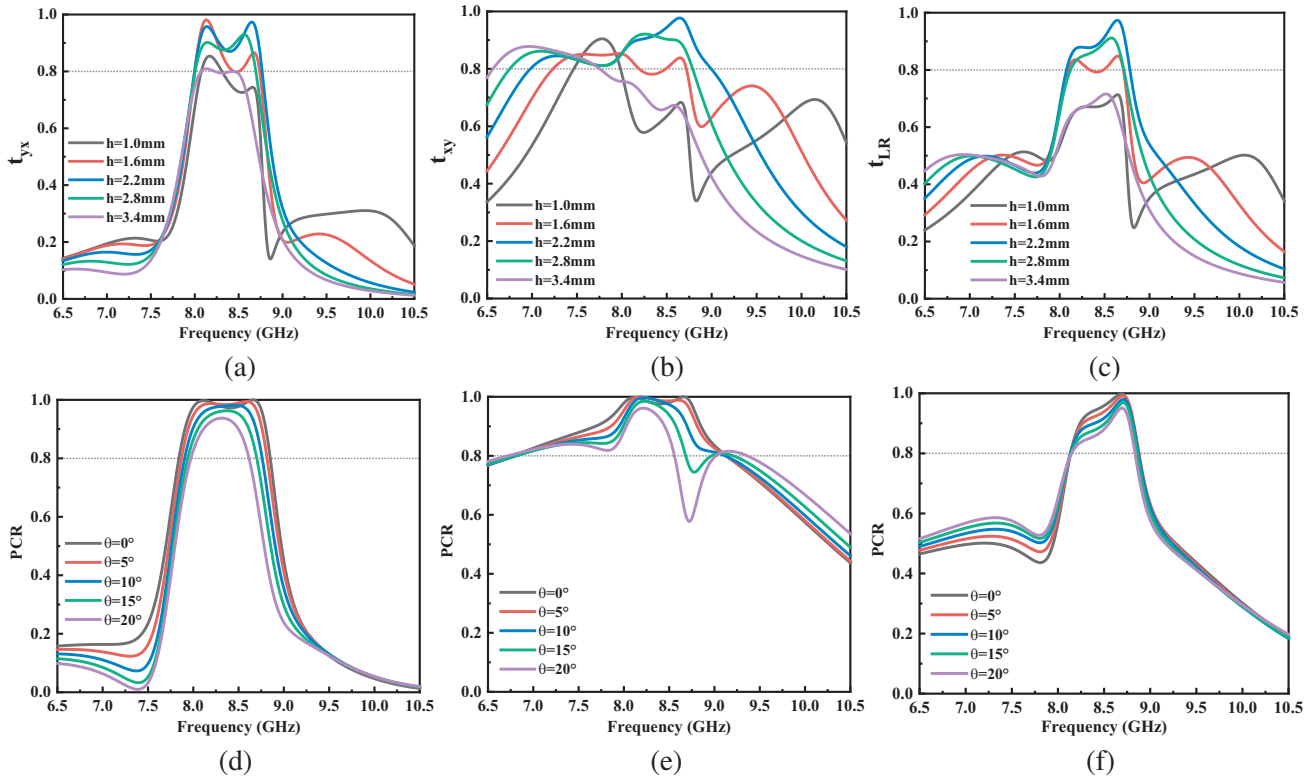

Figure 6. The performance effect of dielectric thickness and incidence angles. (a) t_{yx}, (b) t_{xy} and (c) t_{LR} at different dielectric thicknesses. Polarization conversion ratio of (d) x-polarization incidence, (e) y-polarization incidence and (f) circular polarization incidence at different incidence angles.

3.6 mm. The minor difference in cross-polarization transmission coefficients reflects the compatibility of the aperture coupling to the dielectric. On the other hand, for y-polarized wave irradiation, the increase in thickness leads to a shift of t_{xy} with reduced amplitude towards lower frequency, implying a weaker coupling energy exchange capability through the copper hole. Because of the stable phase state, the simulated cross-polarization transmission coefficients for circular polarization in 8.2–8.9 GHz are only lightly affected at appropriate thickness. To satisfy the low-profile design, the thickness was determined to be 2.2 mm in view of the available substrate.

Subsequently, the case of oblique incidence was also considered. Figs. 6(d), (e), (f) show the PCRs' magnitude of the x-polarization, y-polarization, and circular polarization which declines as the incidence angle increases. Despite the top and bottom asymmetric chiral structures, the meta-device can accept oblique incidence within the operating passband. This is not mentioned in the articles with a similar function.

3. EXPERIMENT AND COMPARISON

To verify the consequences of the implemented theoretical analysis and substantiate the simulation data, a sample of the designed transmissive metasurface is fabricated and tested. The sample consists of 22×22 mateparticles and occupies a total area of $321.2 \times 321.2\,\text{mm}^2$, which is manufactured by the standard print circuit board (PCB) technique in Fig. 7(a).

The experimental setup is shown in Figs. 7(b) and (c). A vector network analyzer (Agilent N5230C)

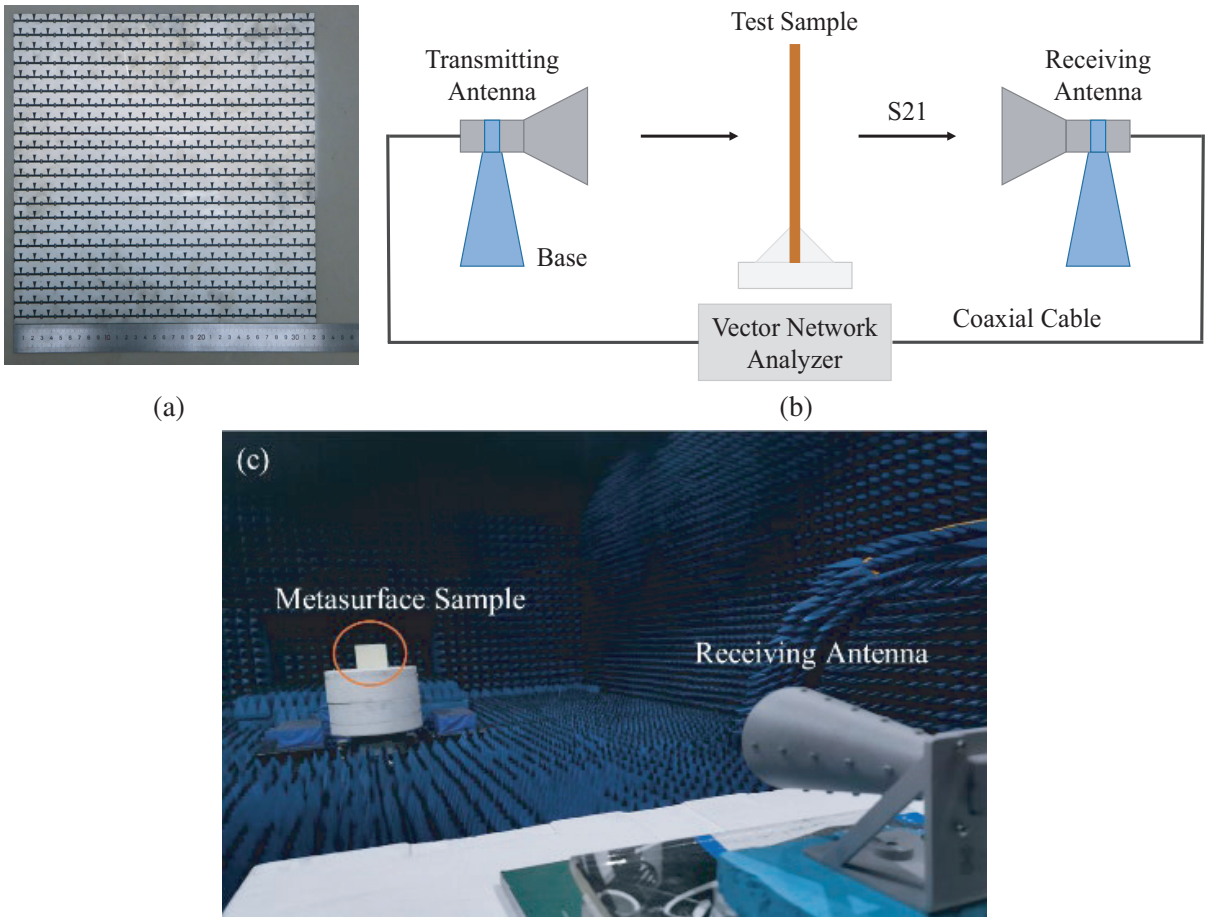

Figure 7. (a) Manufactured sample of the proposed MPC-TMS, (b) experimental setup, (c) test environment.

is linked to the antennas in measurement. Firstly, as the transmitting and receiving antennas, standard pyramidal horn pairs are installed face to face, and the free-space test data serves as the calibration sample. Secondly, the metasurface is located between the antennas vertically, and the co-polarization transmission results are recorded. Thirdly, the receiving antenna is pivoted by 90 degrees without skewing its phase center to acquire linear cross-polarization transmission results. Lastly, standard conical horn antenna pairs with contrary handedness are employed to replace the primal antennas pairs to attain the circular cross-polarization transmission results.

The experimental results are illustrated in Fig. 8. A comparison between the simulated and experimental transmission coefficients for the interaction of the metasurface with the illuminated linear polarization waves is shown in Fig. 8(a). One can see that the trend of measured coefficients curves is consistent with the numerical data over the frequency passband of interest. The cross-polarization transmission peak is almost near unit for both x-polarized and y-polarized incidences with slight frequency discrepancies. Similarly, Fig. 8(b) compares simulated and tested cross-/co-polarization transmission coefficients of circularly polarized incidence. It proves that the magnitudes of experiment coefficients are in qualitative agreement with theoretical results except for the small central frequency shifting. Due to the small ratio of the unit size to the wavelength, manufacturing inaccuracies and

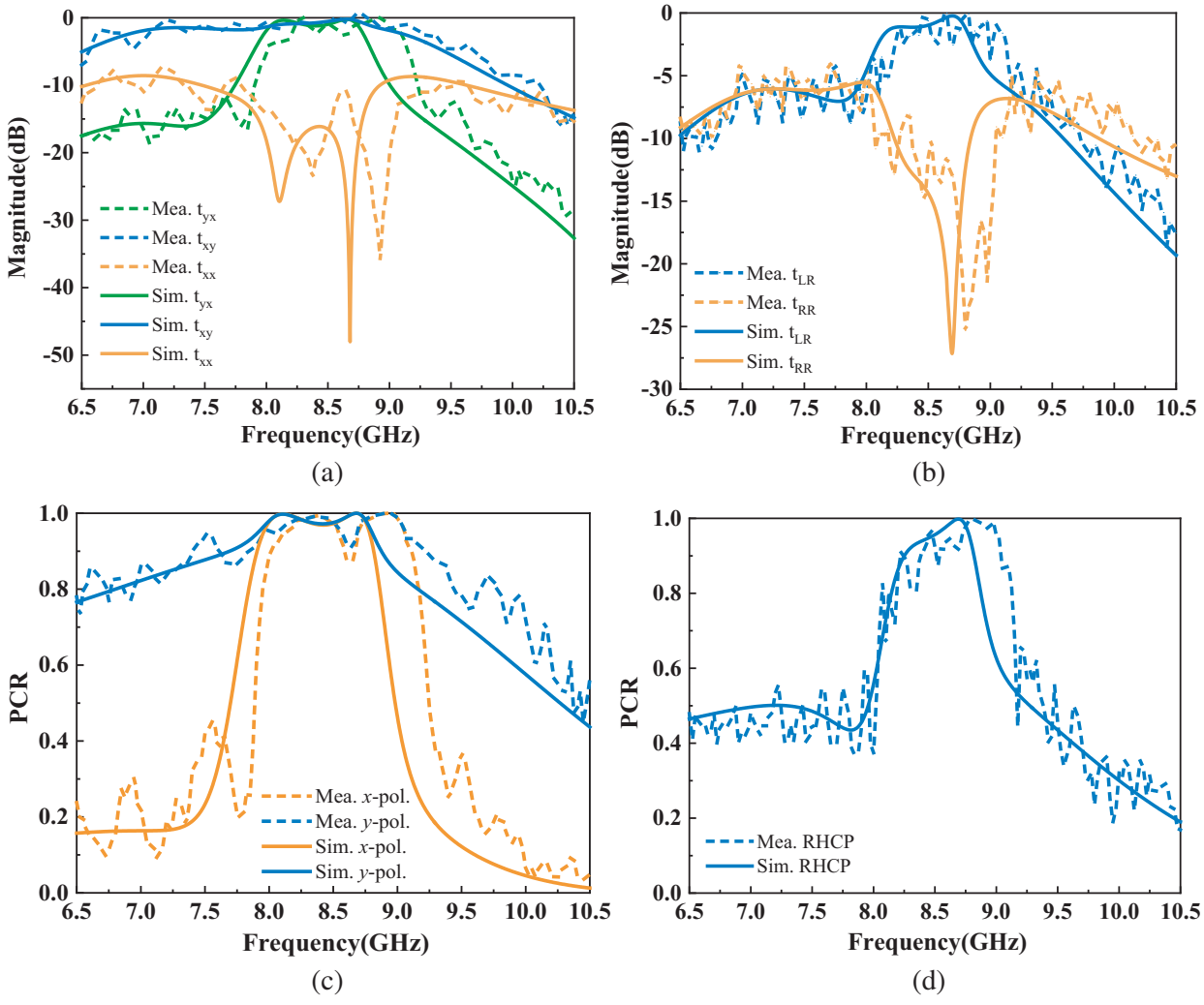

Figure 8. Simulated and experimental results. Transmission coefficients of (a) linear polarization incidence, (b) circular polarization incidence. PCRs of (c) linear polarization incidence, (d) circular polarization incidence.

experimental errors may lead to a shifted resonant frequency. In addition, testing surrounding and device calibration in the lab may affect the harmonic generation, while the total trend sanely coincides with the simulation data. Furthermore, the PCRs for x-/y-polarization and RHCP incident fields are calculated and shown in Figs. 8(c) and (d) based on the measured results. With peak values near unit, the total tendency of PCRs reasonably coincides with the simulation ones, suggesting effective conversion performance.

Various comparisons with transmission polarization converters in previous reports are given in Table 1. What is obvious is that this multifunction microstructure we proposed not only has a simple construction with an ultra-thin thickness, but also reveals superiorities in bandwidth, transmission, and efficiency.

Table 1. Comparison of this design with transmission polarization converters.

Ref.	Mode	Thickness	Bandwidth	Peak T	PCR
[19]	LP to LP	0.06λ	8.79 GHz	0.99	Not given
[32]	LP to CP	0.5λ	8.75–11.25 GHz (25%)	0.95	Not given
[22]	LP to LP LP to CP	0.09λ	7.31–10.58 GHz (36.6%) 14.26-17.36 GHz (19.6%)	< 0.6	$> 99\%$
[33]	CP to CP	0.06λ	10 GHz	0.85	Not given
[26]	CP to CP	0.06λ	5.9 GHz	0.97	Not given
[25]	LP to LP CP to CP	4.18λ	9.0–11.9 GHz (26.4%)	0.95	$> 95\%$
[27]	LP to LP CP to CP	0.1λ	2.17–2.24 THz (3.14%)	0.90	$> 95\%$
[34]	LP to LP CP to CP	0.08λ	15.8–16.7 GHz (5.53%)	0.92	$> 99\%$
This work	LP to LP CP to CP	0.06λ	8.04–8.82 GHz (9.25%) 8.04–9.07 GHz (25.19%) 8.16–8.87 GHz (8.46%)	0.97 0.97 0.95	$> 97\%$

4. CONCLUSION

In summary, a high-efficiency multifunction cross-polarization converter based on transmissive metasurface (MPC-TMS) has been proposed and experimentally investigated. A background of cross polarization is analyzed. The numerical results illustrate that the microstructure can convert x- and y-polarized linearly incident waves into cross-polarized counterparts in 8.04–8.82 GHz (9.25%) and 7.04–9.07 GHz (25.19%), respectively. In the joint passband of 8.16–8.87 GHz (8.46%), the handedness of a circular-polarization plane wave can be concurrently rotated to its opposite. Moreover, resonance superposition and coupling effect have been discussed to study the operating mechanism and parameters influence, which enable similar functions to be implemented in other frequency bands by altering the size. The thickness of the sample is about 0.06λ, while peak transmission and PCR exceed 0.95, demonstrating its advantages compared with related ones. Despite a tiny slight frequency shift, the experimental data are sensibly compatible with the results of simulated calculations. If further researches are steered on this article, a reconfigurable metasurfaces polarization converter may be developed in broadband, multi-band, and arbitrary control. Due to its low profile and insertion loss, this converter is potentially conducive to orbital angular momentum wave generation and satellite communications where polarization diversity is needed.

ACKNOWLEDGMENT

This work was supported by the National Natural Science Foundation of China (No. 61871396).

REFERENCES

1. Doumanis, E., G. Goussetis, J. L. Gomez-Tornero, R. Cahill, and V. Fusco, "Anisotropic impedance surfaces for linear to circular polarization conversion," *IEEE Trans. Antennas Propag.*, Vol. 60, No. 1, 212–219, 2012.
2. Zhao, J., J. Song, Y. Zhou, R. Zhao, and J. Zhou, "Dual-polarization, tunable breaking window in the polarization conversion pass band in a terahertz dirac semimetal-based metamaterial," *IEEE Photon. J.*, Vol. 11, No. 6, 1–9, 2019.
3. Fernandez, O., A. Gomez, J. Basterrechea, and A. Vegas, "Reciprocal circular polarization handedness conversion using chiral metamaterials," *IEEE Antennas Wireless Propag. Lett.*, Vol. 16, 2307–2310, 2017.
4. Jiang, X., Z. Zhang, Y. Li, and Z. Feng, "A planar wideband dual-polarized array for active antenna system," *IEEE Antennas Wireless Propag. Lett.*, Vol. 13, 544–547, 2014.
5. Van Den Broek, G. and J. Van Der Vooren, "On the reflection properties of periodically supported metallic wire gratings with rectangular mesh showing small sag," *IEEE Trans. Antennas Propag.*, Vol. 19, 109–113, 1971.
6. Liu, W., Y. Li, Z. Zhang, and Z. Feng, "A bidirectional array of the same left-handed circular polarization using a special substrate," *IEEE Antennas Wireless Propag. Lett.*, Vol. 12, 1543–1546, 2013.
7. Zhou, H., W. Hong, L. Tian, and M. Jiang, "A Polarization-rotating SIW reflective surface with two sharp band edges," *IEEE Antennas Wireless Propag. Lett.*, Vol. 15, 130–134, 2016.
8. Arnieri, E., F. Greco, L. Boccia, and G. Amendola, "A SIW-based polarization rotator with an application to linear-to-circular dual-band polarizers at K-/Ka-band," *IEEE Trans. Antennas Propag.*, Vol. 68, No. 5, 3730–3738, 2020.
9. Muhammad, S. A., R. Sauleau, L. Le Coq, and H. Legay, "Self-generation of circular polarization using compact Fabry-Perot cavity antennas," *IEEE Antennas Wireless Propag. Lett.*, Vol. 10, 907–910, 2011.
10. Xie, P., G. Wang, H. Li, J. Liang, and X. Gao, "Circularly polarized Fabry-Perot antenna employing a receiver-transmitter polarization conversion metasurface," *IEEE Trans. Antennas Propag.*, Vol. 68, No. 4, 3213–3218, 2020.
11. Pitilakis, A., O. Tsilipakos, F. Liu, K. M. Kossifos, A. C. Tasolamprou, D.-H. Kwon, M. S. Mirmoosa, D. Manessis, N. V. Kantartzis, C. Liaskos, M. A. Antoniades, J. Georgiou, C. M. Soukoulis, M. Kafesaki, and S. A. Tretyakov, "A multi-functional reconfigurable metasurface: Electromagnetic design accounting for fabrication aspects," *IEEE Trans. Antennas Propag.*, Vol. 69, No. 3, 1440–1454, 2021.
12. Shen, C., R. Xu, J. Sun, Z. Wang, and S. Wei, "Metasurface-based holographic display with all-dielectric meta-axilens," *IEEE Photon. J.*, Vol. 13, No. 5, 1–5, 2021.
13. Kato, Y., S. Morita, H. Shiomi, and A. Sanada, "Ultrathin perfect absorbers for normal incident waves using dirac cone metasurfaces with critical external coupling," *IEEE Microw. Wireless Compon. Lett.*, Vol. 30, No. 4, 383–386, 2020.
14. Zhou, G.-N., B.-H. Sun, Q.-Y. Liang, Y.-H. Yang, and J.-H. Lan, "Beam-deflection short backfire antenna using phase-modulated metasurface," *IEEE Trans. Antennas Propag.*, Vol. 68, No. 1, 546–551, 2020.
15. Murugesan, A., D. Natarajan, and K. T. Selvan, "Low-cost, wideband checkerboard metasurfaces for monostatic RCS reduction," *IEEE Antennas Wireless Propag. Lett.*, Vol. 20, No. 4, 493–497, 2021.

16. Dalgac, S., M. Bakir, F. Karadag, M. Karaaslan, O. Akgol, E. Unal, and C. Sabah, "Microfluidic sensor applications by using chiral metamaterial," *Modern Physics Letters B*, Vol. 34, No. 5, 2020.
17. Dalgac, S., M. Bakir, F. Karadag, E. Unal, M. Karaaslan, and C. Sabah, "Characterization of chiral metamaterial sensor with high sensitivity," *Optik*, Vol. 202, 2020.
18. Dalgac, S., F. Karadag, M. Bakir, O. Akgol, E. Unal, and M. Karaaslan, "Chiral metamaterial-based sensor applications to determine quality of car lubrication oil," *Transactions of the Institute of Measurement and Control*, Vol. 43, No. 7, 1640–1649, 2021.
19. Xu, P., W. X. Jiang, S. Y. Wang, and T. J. Cui, "An ultrathin cross-polarization converter with near unity efficiency for transmitted waves," *IEEE Trans. Antennas Propag.*, Vol. 66, No. 8, 4370–4373, 2018.
20. Gao, X., X. Han, W.-P. Cao, H. O. Li, H. F. Ma, and T. J. Cui, "Ultrawideband and high-efficiency linear polarization converter based on double V-shaped metasurface," *IEEE Trans. Antennas Propag.*, Vol. 63, No. 8, 3522–3530, 2015.
21. Murtaza, M., A. Rashid, and F. A. Tahir, "A highly efficient low-cost reflective anisotropic metasurface for linear to linearly cross- and circular-polarization conversion," *Microw. Opt. Technol. Lett.*, Vol. 63, No. 5, 1346–1353, 2020.
22. Han, B., S. Li, X. Cao, J. Han, L. Jidi, and Y. Li, "Dual-band transmissive metasurface with linear to dual-circular polarization conversion simultaneously," *AIP Advances*, Vol. 10, No. 12, 2020.
23. Meng, C., P. C. V. Thrane, F. Ding, J. Gjessing, M. Thomaschewski, C. Wu, C. Dirdal, and S. I. Bozhevolnyi, "Dynamic piezoelectric MEMS-based optical metasurfaces," *Science Advances*, Vol. 7, No. 26, 2021.
24. Cheng, Y. Z., W. Y. Li, and X. S. Mao, "Triple-band polarization angle independent 90 degrees polarization rotator based on Fermat's spiral structure planar chiral metamaterial," *Progress In Electromagnetics Research*,Vol. 165, 35–45, 2019.
25. Song, K., Z. Su, S. Silva, C. Fowler, C. Ding, R. Ji, Y. Liu, X. Zhao, and J. Zhou, "Broadband and high-efficiency transmissive-type nondispersive polarization conversion meta-device," *Opt. Mater. Express*, Vol. 8, No. 8, 2018.
26. Wang, S.-Y., W. Liu, and W. Geyi, "A circular polarization converter based on in-linked loop antenna frequency selective surface," *Appl. Phys. B*, Vol. 124, No. 6, 2018.
27. Cui, Z. T., Z. Y. Xiao, M. M. Chen, F. Lv, and Q. D. Xu, "A transmissive linear polarization and circular polarization cross polarization converter based on all-dielectric metasurface," *J. Electron. Mater.*, Vol. 50, No. 7, 4207–4214, 2021.
28. Fei, P., G. A. E. Vandenbosch, W. H. Guo, X. Wen, D. Xiong, W. Hu, Q. Zheng, and X. Chen, "Versatile cross-polarization conversion chiral metasurface for linear and circular polarizations," *Adv. Opt. Mater.*, Vol. 8, No. 13, 2020.
29. Menzel, C., C. Rockstuhl, and F. Lederer, "Advanced Jones calculus for the classification of periodic metamaterials," *Phys. Rev. A*, Vol. 82, No. 5, 2010.
30. Naseri, P., F. Khosravi, and P. Mousavi, "Antenna-filter-antenna-based transmit-array for circular polarization application," *IEEE Antennas Wireless Propag. Lett.*, Vol. 16, 1389–1392, 2017.
31. Wang, S. Y., W. Liu, and W. Geyi, "Dual-band transmission polarization converter based on planar-dipole pair frequency selective surface," *Sci. Rep.*, Vol. 8, No. 1, 3791, 2018.
32. Xie, P., G. M. Wang, H. P. Li, J. G. Liang, and X. J. Gao, "Circularly polarized Fabry-Perot antenna employing a receiver-transmitter polarization conversion metasurface," *IEEE Trans. Antennas Propag.*, Vol. 68, No. 4, 3213–3218, 2020.
33. Akram, M. R., M. Q. Mehmood, X. D. Bai, R. H. Jin, M. Premaratne, and W. R. Zhu, "High efficiency ultrathin transmissive metasurfaces," *Adv. Opt. Mater.*, Vol. 7, No. 11, 2019.
34. Yu, Y. Z., F. J. Xiao, I. D. Rukhlenko, and W. R. Zhu, "High-efficiency ultra-thin polarization converter based on planar anisotropic transmissive metasurface," *AEU — Int J. Electron. C.*, Vol. 118, 2020.